DESIGN REQUIREMENTS AND OPTIONS FOR FINAL FOCUSING SUPERCONDUCTING MAGNETS OF HEAVY-ION DRIVERS

L. BROMBERG* *MIT Plasma Science and Fusion Center, 77 Massachusetts Avenue Cambridge, Massachusetts 02139*

ARIES-IFE TEAM

Received June 1, 2003
Accepted for Publication April 29, 2004

The environment close to the chamber of heavy ion inertial fusion energy reactors imposes severe constraints on magnets used for final focusing magnets. Space is at a premium, requiring close proximity of adjacent magnets, making magnet integration imperative. In addition, the high radiation flux imposes stringent shielding requirements. In this paper, the options for final focusing magnet topologies are described. Implications of using both high-temperature superconductors and conventional low-temperature superconductors are investigated. The use of high-temperature superconducting materials may offer an attractive, although speculative, opportunity for a fundamentally different approach to magnet construction, leading to either lower cost or reduced maintenance.

KEYWORDS: *inertial fusion energy, final optics magnets, focusing magnets*

I. INTRODUCTION

The final focusing magnets for the heavy ion driver for inertial fusion present design challenges. The magnets are quadrupoles, used for final focusing of beam arrays. Because of space requirements, it is necessary to pack them in as tight an array as possible. In this configuration, adjacent magnets interact with each other electromagnetically, structurally, and thermally.

Because of the close contact between them, it is interesting to explore design concepts that exploit this feature. Quadrupole magnet arrays can be optimized beyond simply assembling the array from individually optimized quadrupole magnets. It is the purpose of this paper to explore this optimization.

The design of fusion magnets has to address the high radiation fields present at the magnets, affecting the superconducting properties of the conductor, the properties of the normal material stabilizer/quench protector, the insulation, and the cooling. The radiation characteristics also are different from those in magnetic fusion because of the pulsed nature of the radiation. This effect impacts the radiation limit for the insulator.

The choice of superconductor affects the characteristics of the magnet array. Low-temperature superconductors (LTSs) are well developed (with thousands of magnets fabricated and operated in particle accelerators). It should be mentioned that before high-temperature superconductor (HTS) magnets are practical, it is necessary to address issues of large-scale fabrication, good current density, and high current capacity of HTS materials, at an affordable cost. One of the purposes of this paper is to evaluate potential advantages of HTSs in the design, manufacture, and operation of final optic magnets for inertial fusion energy (IFE) if these hurdles can be overcome.

In this paper, the design options for final focusing magnet arrays are discussed. The restrictions imposed on optimized, aggressive high-temperature quadrupole final focusing magnets operating at elevated temperatures are discussed. Short sample properties of the HTS materials are used, as well as epitaxial deposition schemes that are in early stages of development. A comparison is then made with optimized quadrupoles that use LTS materials.

II. QUADRUPOLE ARRAY DESIGN OPTIONS

The design of quadrupole arrays, especially those that need a high density of quadrupoles, has different

*E-mail: brom@psfc.mit.edu

requirements from those of individual quadrupoles.[1] There is extensive experience with the latter because of their use in particle physics accelerators. Low-temperature superconducting quadrupole arrays have been investigated, including cryogenic, structural, and superconducting issues for a particular case.[2–8] In this section, the options for the design of quadrupole magnet arrays are generalized.

II.A. Magnetic Field Calculations

The scalar potential description of the magnetic field is

$$\boldsymbol{B} = -\nabla\phi \ , \tag{1}$$

where **B** is the magnetic field and ϕ is the scalar potential. This description is applicable when the volume is void of currents, when it can be shown that the above scalar potential has to satisfy Laplace's equation,

$$\nabla^2\phi = 0 \ . \tag{2}$$

The design of quadrupole arrays requires the application of the boundary conditions. However, it is instructive to solve Eq. (2) first and then find the boundary conditions that apply for the different solutions.

The solution of Laplace's equation with appropriate poloidal angle dependence in cylindrical coordinates is

$$\phi = \Sigma(\sin(m\theta)(A_{1,m}r^m + B_{1,m}r^{-m}) + \cos(m\theta)(A_{2,m}r^m + B_{2,m}r^{-m})) \ , \tag{3}$$

where θ is the poloidal angle and r is the radius from the center of the cell. The sum is for $m > 0$. Since the solution needs to be finite at $r = 0$, only solutions with $B_{1,m} = B_{2,m} = 0$ are allowed.

For a quadrupole field structure, $m = 2$, and therefore, the solution for the scalar potential is

$$\phi = A_1 r^2 \sin(2\theta) + A_2 r^2 \cos(2\theta) \ . \tag{4}$$

The solution with $A_1 = 0$ will be referred to as the cosine quadrupole, while the solution with $A_2 = 0$ will be referred to as the sine quadrupole. There could be linear superposition of the two solutions, but in practice only one or the other is of interest.

Figure 1 shows the field profile for the quadrupole array for both the sine and cosine solutions. In the sine quadrupole case, the magnetic field in the region close to the boundary has substantial components parallel to the boundary between cells, while in the cosine quadrupole case, the magnetic field is only perpendicular to this boundary. Again, cells need to be located next to each other because of space limitation at the location of the final focusing magnets.

It should be noted that at any point the heavy ion beam is elongated/compressed in the direction perpendicular to the local magnetic field. In the case of the cosine quadrupole, the axes of the ellipse formed by the beam cross section are aligned with the diagonals of the cell, while in the case of the sine quadrupole, they are aligned normal to the boundaries of the cell. Therefore, the cosine quadrupole may offer geometric advantages of reduced beam scraping.

If the beam apertures are made circular, the closest packing can be obtained not by using an arrangement in a square matrix, as shown in Fig. 1, but instead using an arrangement in a hexagonal, honeycomb-like pattern ($m = 3$). However, since the field pattern is "square" looking ($m = 2$), the use of a square pattern is a more natural one and results in a better match between the required field structure and the magnet arrangement.

Because of the different field profile in the cell, the current density at the boundary between cells is different for the cosine and sine quadrupoles. By using symmetry as shown in Fig. 1, it is straightforward to calculate the surface current density required to produce the magnetic field. The surface current density K is determined by

$$K = \Delta B/\mu_0 \ , \tag{5}$$

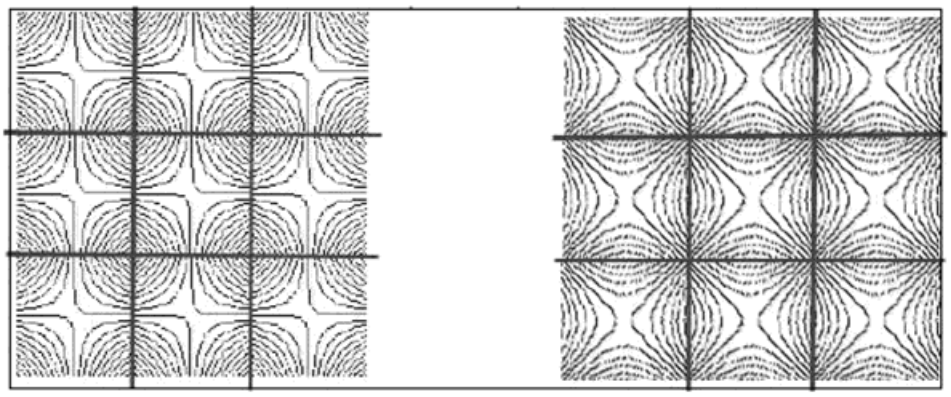

Fig. 1. Field profiles for cosine and sine quadrupole arrays.

where $\Delta B = (B_1 - B_2)$, and B_1 and B_2 are the values of the magnetic fields parallel to the surface at opposite sides of the boundary. The field perpendicular to the surface is continuous because of the divergence-free nature of magnetic fields. The surface current density is in the direction perpendicular to the fields, directed along the surface and aligned with the axis of the focusing magnet.

For the cosine quadrupoles, the surface current density is given by

$$|K_{cosine,\,x\text{-}wall}| = 4A_1 x/\mu_o \quad \text{for } -a < x < a \qquad (6)$$

on the x-wall and

$$|K_{cosine,\,y\text{-}wall}| = 4A_1 y/\mu_o \quad \text{for } -a < y < a \qquad (7)$$

on the y-wall. Here, a is the half-width of the cell, and A_1 is a constant. The current therefore reverses on each face. The current density is not uniform but increases linearly starting at the center of each face, but in opposite directions.

For the sine quadrupole, the current density in each face is uniform, given by

$$|K_{sine}| = 4A_2 a/\mu_o \ . \qquad (8)$$

In this case, the net current in each face of the quadrupole is not zero, and therefore, the current needs to be balanced by returning the current that flows in one face through the adjacent faces. The current distribution for the cosine and sine quadrupole arrays is shown in Fig. 2.

In both the sine and cosine quadrupoles, the total magnetic field is given by

$$|B| = 2Ar \ , \qquad (9)$$

and the gradient of the magnetic field magnitude is

$$d|B|/dr = 2A \ . \qquad (10)$$

The above discussion does not address the issues of fields at the ends of the quadrupole or at the edge of the array, which introduce errors. Flux termination issues are addressed in Sec. V.

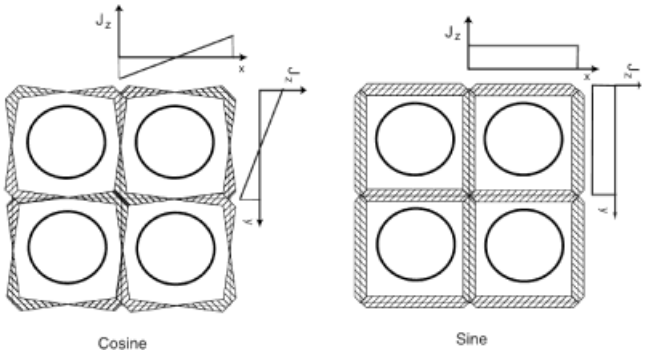

Fig. 2. Current distribution in planar cosine and sine quadrupoles. Different hatch patterns indicate different current direction (out-of-page and into-page).

II.B. Force Considerations

In this section, the forces in the quadrupole arrays for the final optics magnets are described. Because of symmetry, it is straightforward to show that the forces are aligned along the cell boundaries, producing only in-plane loads. Although this is the ideal case, care must be taken in the detail design to ensure that the loads are aligned. The in-plane loads have two components: a transverse load (perpendicular to the main axis of the plate) and a longitudinal force (along the main axis of the plates).

The forces in the quadrupoles are complex because of the ends. The longitudinal loads are exclusively generated by the quadrupole ends. They are also aligned on the planes of the cell boundaries. However, the longitudinal loads due to the ends are relatively small compared with the transverse ones and are ignored in the discussions below, which are meant more for scoping studies than for detailed design.

The forces due to the axial current flowing in quadrupole arrays can be easily calculated using the analytical solution for the planar quadrupole obtained in Sec. II.A. For both sine and cosine quadrupoles, the integrated transversal force per unit length is given by

$$F = 4A^2 a^3/\mu_o \ , \qquad (11)$$

and the value of the associated transverse stresses is given by

$$\sigma = F/t \ , \qquad (12)$$

where t is the thickness of the structural plate.

Even though the force magnitudes are equal, there is a fundamental difference between the sine and the cosine quadrupoles. While the cosine quadrupole has a tensile load across the narrow dimension of the plane of the quadrupole, the sine quadrupole has a compressive load. The load support is determined not only by the intrinsic properties of the structural material strength but also by buckling considerations.

It is possible to prevent tension in the structure for the case of the cosine quadrupole by preventing the load path from going through the center of the plate (for example, by making a slit through the middle of the flat plate). In this case, the loads need to be reacted by the adjacent plate, which also has a force equal in magnitude but opposite in direction. As in the case of the sine quadrupole, care needs to be taken to prevent buckling of the plates when in compression.

The design requirement for the structural material also needs to meet strain limitations of the superconductor. To limit strain in the superconductor to 0.2% (HTS strain limitations are comparable to those of LTSs), the maximum tensile stress in the structure is ~500 MPa.

Compressive stresses are comparable but for our case are limited by buckling.

II.C. Stored Energy

In order to provide the quench protection required for LTS, it is necessary to determine the stored magnetic energy in the quadrupoles. For both magnet topologies with flat plates, the energy per quadrupole is given by

$$E = 16A^2a^4L/3\mu_o \ ,$$

where l is the length of the quadrupole. Typical numbers are ~200 kJ/magnet. An array of about 100 magnets would therefore store ~20 MJ. It may be possible to connect all the magnets in the array in a series configuration. Assuming a 2500-A conductor, the dump time for 20 kV would be approximately several seconds. Higher currents result in shorter dump times but would require larger cross sections. It may be necessary to electrically divide the quadrupole array to provide faster energy dump. The dump time determines the amount of copper stabilizer required for the case of quench protection in LTSs.

II.D. Configuration Considerations for Planar Quadrupole Magnet Arrays

The planar quadrupole magnets that are attractive for the final focusing magnet arrays have current density distributions that are different from that of individual quadrupoles, as indicated above. Their design should address this difference, as done by Martovetsky et al.[9]

The options for manufacturing the planar elements that make up a quadrupole in an array are shown in Fig. 2. For the case of the cosine quadrupoles, the magnet can be made from flat plates, one for each boundary between cells. These flat plates carry no net current. The plates can be placed in a structural grid to provide appropriate positioning ("keying") of the individual flat plates. As indicated in Sec. II.B, the net load in the plates is zero (by symmetry), and the loads are all in the plate direction (resulting in no requirement of out-of-plane loads, which need to be supported by bending). The outer cells elements, which do not have a corresponding balancing element, need to be supported externally. Outer cell issues are discussed in Sec. V.

In contrast, the sine quadrupole has the current in the same direction in each plate. Therefore, the electrical requirements of net zero current in each element (so that the current in the leads can be small) indicate that a different approach must be taken. There are two ways to implement this solution, as shown in Fig. 3. In the first one, each quadrupole is made of two sections, using 90-deg angle elements. In this manner, the current on one of the plates making the 90-deg angle element is returned in the other plate of the angle element. In this case, with two 90-deg angle elements per quadrupole as shown in Fig. 3a, the net forces in each of the plates are zero, by symmetry.

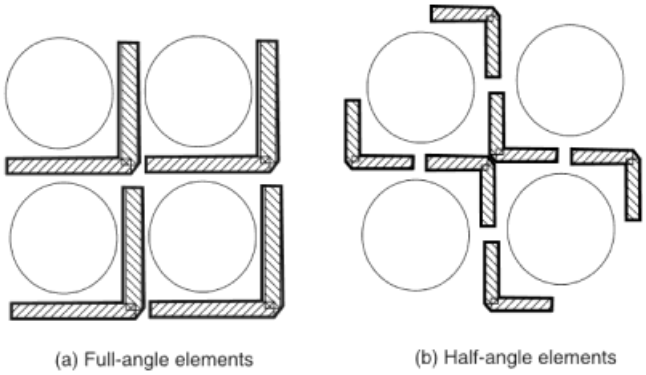

Fig. 3. Options of sine quadrupole arrangement made of (a) full-angle elements and (b) half-angle elements. Different shading indicates current orientation (into-page or out-of page).

Each angle of the plates, however, experiences large compressive stresses that need to be supported against buckling, as described above. In this case, the number of full-angle elements required in the quadrupole array is approximately the same as the number of quadrupoles in the array since the elements are shared.

An alternative method of implementing this geometry would involve making each quadrupole out of four separate half-angle segments, as shown in Fig. 3b. In this case, although the fields are shared, it is necessary for each quadrupole to have four elements. The adjacent quadrupoles need to have their own 90-deg angle elements as shown in Fig. 3b. Winding considerations of the superconductor in the plates is covered in Sec. III.C.

III. DESIGN REQUIREMENTS FOR QUADRUPOLE MAGNET ARRAYS

Superconductors have four design requirements that must be considered when they are used in nuclear applications: (a) survival of the insulation, (b) the stabilizer and (c) the superconductor under irradiation, and (d) removal of nuclear heating. In this section, these requirements are summarized, and their impact on the HTS options is reviewed.

III.A. Insulation

Organic insulators have substantially lower fluence life than inorganic insulators. This is because organic insulators are limited by chemical changes due to bond breaking, while for inorganic insulators the life is determined by swelling caused by gas generation by nuclear process or damage to the crystallographic structure of the material.

In organics, the bond breaking can be described in terms of *g* values, or the number of radicals, atoms, or bonds broken per 100 eV of absorbed energy. Since the mechanisms for different types of irradiation are similar, the *g* values from these different forms of radiation are comparable. Therefore, the relevant number for characterizing irradiation damage from neutrons, gammas, and electrons is in terms of energy density dissipated in the material, or grays. For organics, both neutrons and gammas cause damage, and fluence life limits are $\sim 10^8$ Gy, even in the absence of shear across the insulation.

The fluence limit for inorganic insulators is determined by swelling. For practical insulators the maximum irradiation ranges from 10^9 to 10^{11} Gy depending on whether the insulator is in sheets or in powder form. The corresponding neutron fluence is 10^{22} to 10^{24} n/m^2.

For IFE final focusing magnets, because of the openings required for transmission of the beam, the radiation for a constant thickness shield is larger than for comparable magnetic fusion energy (MFE) concepts, and the spectrum and the nature of the radiation are also different. Table I shows the neutron and gamma maximum insulator fluences assuming a machine with 40 full-power years (FPY). Three locations are shown for the ARIES-AT design, while the radiation to the insulator of the final focusing magnet is shown for varying thicknesses of the beam-flibe distance. Not only are the values much larger for the final focusing magnets than they are for ARIES-AT, but also the ratio between gammas and neutrons is very different. The gamma fluence is a factor of $\sim$6 larger than the neutron fluence, while for ARIES-AT the neutron and gamma fluences are comparable. This is because of the lack of neutron capture materials that tend to decrease the neutron flux and the gamma-ray generation rate close to the magnets.

Not only can the neutron/gamma distribution differ between IFE and tokamak applications, but also the dose rate is extremely different. While for magnetic fusion applications the dose rate is nearly constant, for IFE the dose rate is pulsed with a very low duty cycle. The radiation pulse in IFE is <1 μs while the pulse rate is about ten times per second. This results in an instantaneous dose rate five orders of magnitude larger than for MFE with equivalent average dose rates.

The effect of dose rate is unknown for the organics that are currently being considered. For very high instantaneous dose rates, it is possible that the radicals/ions/atoms generated interact with each other because of their much higher density. It has been mentioned that damage to organic insulators is due to changes in chemistry. High dose rates result in a large concentration of radicals generated in the radiation, which could recombine with each other (increasing gas generation). On the other hand the data from aging of irradiation indicate that at lower radiation dose rates, the insulation damage is greater.[10]

Present-day testing in TRIGA reactors results in a dose rate of $\sim$300 Gy/s. The average dose rate for aggressive IFE designs is on the order of 1 Gy/s, with an instantaneous dose of $\sim$0.1 MGy/s. For comparison, the average dose rate for ARIES-AT is $\sim$0.25 Gy/s. Therefore, the present testing rate is accelerated for magnetic fusion (by a factor of $\sim$1000) but is slow compared to the instantaneous dose rate in inertial fusion (by a factor of $\sim$300).

From these discussions it is clear that the final focus magnets could benefit, although only slightly, from the use of inorganic insulation. Not only are the limits of this type of insulation higher than radiation-resistant organic insulators, but also inorganic insulators are not sensitive to gamma rays. Present-day data on high-performance organic insulators indicate the feasibility of utilizing organics up to a few times 100 MGy (Ref. 11).

TABLE I

Neutron, Gamma, and Total Fluences for Illustrative Tokamak (ARIES-AT) and Calculated for IFE Final Focus Magnets, 40 FPY, Polyimide Insulation

	Neutrons	Gammas	Total
ARIES-AT			
Inboard	41	33	74
Divertor	31	26	57
Outboard	50	320	370
IFE-flibe			
1-cm gap	380	2480	2860
0-cm gap	100	600	700

*The fluences are in Mgrays.

III.B. Stability/Quench Protection

High-temperature superconductors do not suffer from flux jumping when operated at temperatures higher than $\sim$10 to 20 K because of the very high thermal capacity of the metals at these temperatures (about two orders of magnitude higher than at 4 K). As a result, there is no need for a substantial fraction of normal conducting material, in contrast with LTS materials. The only normal conducting material required is whatever is needed to manufacture the superconductor. In the case of YBCO, it is a nickel tape. For BSCCO, the filaments are likely to be placed in a silver matrix.

The high thermal capacity of HTS materials increases the difficulty of quench detection, mainly because the quench zone propagates very slowly in HTSs. For active magnet protection, novel methods of quench protection and quench detection would be required for HTSs at high temperatures. Since either passive or active quench protection is difficult in HTS magnets, an alternative approach is suggested. Because of the very large source of energy required to start a quench in an HTS magnet, it is assumed that flux jumping and quenching

do not occur. As a consequence, for the HTS design it is assumed that all of the stabilizer and quench protection normal conductor could in principle be eliminated from the coil.

At present the engineering current densities of HTS conductors are low because of the silver matrix for BSCCO and the nickel substrate for YBCO. In this paper the implications of a successful development program for reduction of the nonsuperconducting fraction of the conductors. For LTSs, stabilization and quench protection are required, and this material is included in the conductor. The radiation damage to the stabilizer/quench protector is assumed to be annealed with periodic warmup of the magnet during scheduled maintenance periods.

III.C. Superconductor

The properties of HTS materials that are of interest in fusion have been recently described and will be only briefly reviewed in this paper.[12,13] HTS materials are ceramic and are therefore brittle in nature. The production of long lengths of wires or tapes suitable for winding magnets has limited the application of HTSs. The solutions developed for manufacturing high-performance A-15 superconductors (such as Nb_3Sn) are being used in the fabrication of HTS wires. In this paper, thick films (of $YBa_2Cu_3O_{7-x}$ compounds, referred to as YBCO) are assumed. However, it should be mentioned that long-length tapes made of this material have yet to be manufactured.[14,15] Short sample properties will be assumed, with the hope that in the future the barriers for manufacturing long lengths of thick tapes and wide areas of YBCO deposition will be overcome.

The measurements of YBCO-123 performance at several temperatures as a function of the magnetic field are shown in Fig. 4 (Ref. 15). These results were obtained for highly textured tapes and show the difference in the behavior of these highly anisotropic superconductors as magnetic fields are applied either perpendicular or parallel to the main plane of the crystal. The performance of YBCO at liquid nitrogen temperature and 10 T is comparable to the noncopper current density of the Nb_3Sn superconductor, at 4 K and 0 T. Indeed, when the structure and stabilizer/quench protection is included in the Nb_3Sn designs, the average current density in the Nb_3Sn conductor is substantially lower than that for YBCO at elevated temperatures.

A large amount of anisotropy exists in the superconductor, depending on whether the field is aligned with the *c* axis or perpendicular to it. The difference is especially large at higher temperatures. For YBCO thick-film conductors, the *c* axis is perpendicular to the tape.

An interesting alternative to the YBCO tapes is to use BSCCO material, 2212, not shown in Fig. 4. This material has good current-carrying capabilities at low temperatures and is easier to manufacture than YBCO (Ref. 16).

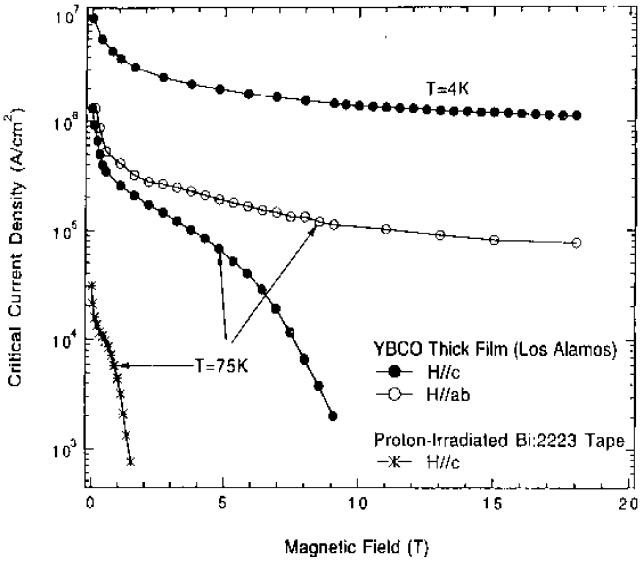

Fig. 4. The critical current density for YBCO-123 as a function of magnetic field for several temperatures and for different field orientations with respect to the crystal (from Ref. 15).

III.D. Superconductor Radiation Damage

The radiation damage to HTS and comparison to LTS for fusion applications has been addressed previously. In this paper, only a brief summary is provided.

The limit of radiation damage to HTSs has not been established yet, with indications that properties improve through neutron fluences in excess of 3×10^{22} n/m^2. It is assumed that their limit is $\sim 10^{23}$ n/m^2, a dose about half an order of magnitude higher dose than that for LTSs (Refs. 17 and 18).

III.E. Nuclear and Alternating-Current Loss Heating

By operating at 50 to 77 K, it is possible to remove the same thermal power using a refrigerator that is ~40 times smaller than if the same thermal power is removed at 4 K. Therefore, neutron, gamma, and alternating-current loss heating of the cryogenic environment ceases to be a constraint for practical designs when HTSs are used.

The choice of operating temperature is important because it impacts the coolant choice. For temperatures lower than ~66 K, the only practical coolant is high-pressure helium gas. For higher temperatures, liquid nitrogen is the coolant of choice.

III.F. Cooling

For the LTS option, usual cooling techniques can be used (pool boiling or cable-in-conduit conductor) using liquid helium.

In order to cool the elements in quadrupole magnet arrays utilizing HTSs, alternatives to the use of a cryogenic fluid need to be developed. This is because there are not appropriate cooling liquids between liquid nitrogen and liquid helium temperature. Hydrogen is undesirable because of explosion problems, and neon is very expensive, although available.

Dry systems can be developed that reduce the amount of liquid required. In order to remove the heat from the bulk of the magnet to the ends, it is possible to allocate a fraction of the cross section to a high-thermal-conductivity element, used to conduct the heat to the ends of the quadrupoles, where it is removed. It is necessary to use a nonstructural element for this purpose since the thermal conductivity of structural elements is usually very small. Figure 5 shows a schematic of the cross section of one of the flat plates used in the cosine quadrupole array design. The edges are made of highly conductive material such as copper.

By utilizing this approach, assuming a volumetric heat load in the magnets of 1 mW/cm^3 and a length of the quadrupole of $\sim$1 m, it is possible to decrease the temperature difference between the center of the magnet and the ends to $\sim$2 to 3 K, with the use of only 5% of the cross-sectional area for the copper. The temperature difference across the plates is substantially smaller than this.

At the ends, the heat must be removed, either by high-pressure helium or by liquid neon.

IV. QUADRUPOLE MAGNET IMPLEMENTATION

In this section, the rules and methods developed in Secs. II and III are used to illustrate the design options. Designs will be presented for a low-temperature material wound from conventional Rutherford cable conductor and for HTS plates made with YBCO thick films. The goal is not to design the best magnet but to illustrate the process.

It is assumed that the HTS magnet is a sine quadrupole arrangement, while the LTS magnet is a cosine quadrupole arrangement. The bore of the magnet is the same, with the same field gradient. The goal is to determine the cell size required for the design.

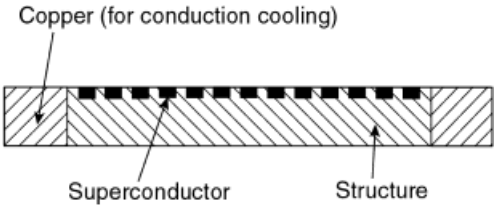

Fig. 5. Illustrative approach for cooling bulk of plate, with high-conductivity material at the edges of the plate for heat removal.

Both designs have the same parameters for the quadrupoles: beam aperture of 0.15 m, beam tube thickness of 0.001 m, thickness of the MLI (cryogenic shielding) of 0.005 m, and thickness of additional shielding/structure of 0.03 m. In addition, it is assumed that the conductor pack has a 0.005-m-thick structural envelope for ease of assembly and to help with buckling constraint and the axial loads. These elements are directly between the superconductor elements and the beam aperture.

IV.A. Low-Temperature Cosine Quadrupole Magnet Design

In the case of the LTS magnet, it is not possible to manufacture the plates or the 90-deg angle elements using epitaxial techniques, and the superconductor needs to be wound in the supporting structure. This limits the options for the manufacture of the flat plates (for cosine quadrupoles) or angle elements (for sine quadrupoles).

For the case of the cosine quadrupoles, the Lorenz loads can be supported through tension across the plate or by compression and balanced reaction by the adjacent element. If supported in tension, the Lorenz forces in each conductor need to be transferred to the structure. For the case of a wound conductor, channels in the structure are needed for transferring these loads.[4] In the case of compression and reaction by the neighboring element, there is no need for transferring these loads to the structure. Supporting the Lorenz loads through tension makes the structure substantially less effective. It is possible to prevent large tensile stresses in the flat plates, as suggested in Sec. II.B, by placing a slit through the middle of the plate and reacting the loads in one-half of the plate to be supported by the adjacent plate that has loads that are equal but opposite in direction. In this manner, the conductor and structure are in compression, and a substantial fraction of the load can be carried by the conductor in compression.

The unit cell is illustrated in Fig. 6. The conductor is probably a Rutherford cable, manufactured by the react and wind technique (if the conductor is Nb_3Sn). The issue of winding at the ends is beyond the scope of this paper. As mentioned above, the cosine quadrupole has a current distribution that varies linearly with distance from the center of the flat element. This can be approximated by placing more conductors in regions away from the center of the flat element, as indicated in Fig. 6. As previously noted, the loads from the conductor are reacted by the next neighbor. In Fig. 6 a positioning and load transferring structure is shown whose purpose is to transfer the loads from one flat element to the opposite one. Of course, each positioning and load transferring structure is associated with both horizontal and vertical elements,

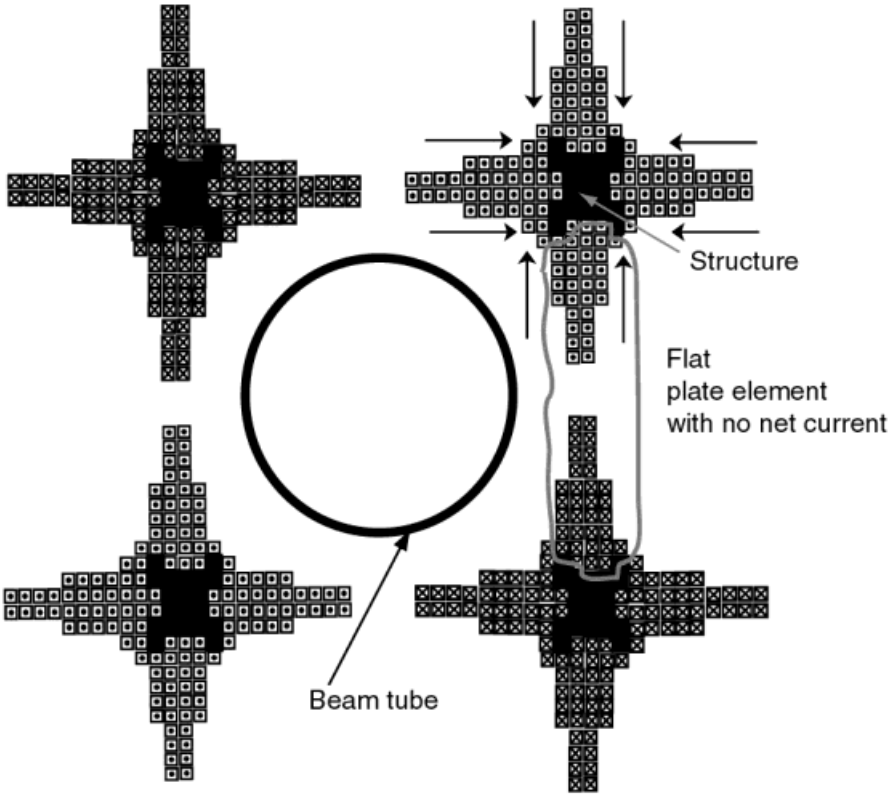

Fig. 6. Illustrative diagram of cell for wound cosine quadrupoles (LTS). Loads generated in opposite sides of plate elements are reacted by antisymmetric forces in adjacent plate elements, not through structures in the plate element.

as indicated in Fig. 6. However, it is emphasized that the flat elements, as indicated in Fig. 6, carry no net current. In other words, the elements behave differently electrically and structurally with currents not being shared but with loads being shared among separate elements.

In the design shown in Fig. 6, the currents in the cross-corner section are all in the same direction. This is unfortunate in that it is not possible to assemble them as a unit prior to installing them in the array but instead must be assembled from elements that when put together form the cross-corner assemblies.

Several values of the field gradient have been used, from an aggressive 40 T/m to a less aggressive 20 T/m. Note that the half-cell dimension does not vary much with varying field gradient. This is because the bulk of the dimension between the beam channel and the cell symmetric plate is determined by constant values of shielding, shielding/structure, and tube diameter. The effect of the thickness of the superconductor is not very important because the superconductor element is thickest in the region where the space is not needed for cryogenic insulation, radiation shielding, or tube diameter, i.e., in the region in the corner of the cells. For the cases illustrated in Table II, the assumed current density in the Nb_3Sn superconductor was chosen to be substantially smaller than is possible. It is assumed that the superconductor

TABLE II

Cosine Quadrupole Using Nb_3Sn Superconductor

Field gradient (T/m)	40	30	20
a (m)	0.197	0.193	0.191
B_{max} (T)	7.9	5.8	3.8
A (T/m)	20	15	10
Current density (MA/m^2)	260	380	540
Current density, noncopper (MA/m^2)	3000	4300	6200
Surface current density (K) (MA/m)	12.5	9.2	6.1
Cosine quadrupole			
Total conductor thickness (cm)	4.8	2.4	1.1
Compressive stress in conductor (MPa)	200	210	200
Beam radius (m)	0.15	0.15	0.15
Field at aperture (T)	6.2	4.5	3.0
Conductor thickness (cm)	0.3	0.25	0.2
Pack current (kA)	2.3	2.4	2.2
Number of layers, maximum	16	10	6
Number of turns per layer, maximum	131	154	191
Stored energy per unit length (MJ/m)	2.60	1.30	0.60

has a copper fraction of 50% and that the structure and cooling of the conductor decreases the average current density by an additional factor of 4 on top of a margin of 70% of current sharing. The current density was chosen so that the compressive stresses in the conductor, excluding the additional structure that can be provided by the shielding material, is ~200 MPa to limit the strain degradation in the conductor. Indeed, it is possible to utilize NbTi for those cases in Table II with field gradients of 30 and 20 T/m.

The cells that are at the outer edges of the array need compensation in order to behave in the manner described here. This can be accomplished by placing an appropriate current distribution in this region in order to simulate the presence of an infinite array of quadrupoles. The current distribution at the edge of the quadrupole array for achieving this effect has been calculated in the past by Thome.[19] In addition, to provide appropriate current distribution, the elements at the outer edge do not have balancing forces from adjacent elements. These loads must therefore be supported by an external structure. Detailed calculations of the outer edge effects are beyond the scope of this paper.

For the case of a cosine quadrupole magnet using HTS materials, the conductor distribution in the plate elements is shown in Fig. 7. This figure illustrates the options for depositing the material for the cosine quad arrays that requires nonuniform current distribution in the plates. The current distribution, which flows antisymmetrically on opposite sides of the plate, can be made by applying a constant thickness conductor with varying spacing, or it can be done with relatively constant spacing but with varying width, or a combination of the two. The current sharing density is relatively uniform since the magnetic field is uniform across the plate.

IV.B. HTS Sine Quadrupole Magnet

For the case of the sine quadrupole arrays, the conductor needs to be placed or deposited on 90-deg angle elements with uniform current density. The loads from the axial conductor are aligned with the plates but point toward the middle of the plates, as previously described in Sec. II.B. Not only is there conductor in the middle of the plates but also the forces are greatest there, requiring most structure (this is not the case in the cosine quadrupole). The radial build of the quadrupole is determined by the thickness of the magnet in the middle of the plates. The most efficient method of supporting these loads is in compression. Therefore, means need to be provided to control buckling.

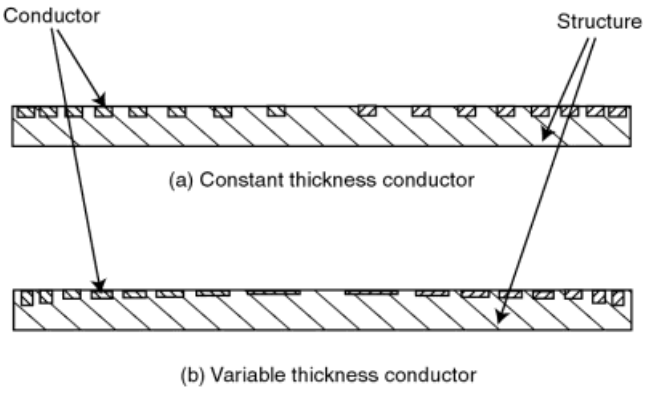

Fig. 7. Design of plates using epitaxially deposited HTS for cosine quad arrays.

In this section, illustrative design parameters of a sine magnet with HTSs are presented. The main beam parameters (field gradient, beam aperture, and thicknesses) are the same as for the LTS magnet described above. The superconductor is now spaced uniformly in the structural 90-deg angles. The loads are supported by compression in the planes that make the half angle, and as before, a 0.005-m structure is used to surround the superconductor pack to ease handling and to address axial loads and buckling.

Table III shows results from the calculations for field gradients similar to those in Table II for LTSs. It should be noted that the cell size (2a) is similar in both designs. The cell size in this case is larger not because of the use of HTS material but because of the use of the sine quadrupole arrangement. In both cases the cell size is on the order of 0.40 m.

Figure 8 shows a schematic diagram of one of the 90-deg angle elements with HTS material. The ends of the element need to be rounded to allow for current transfer from one plane of the angle element to the other.

An advantage of this design over the cosine quadrupole design is that the corner elements can be assembled remotely and inserted because of the zero net current of these elements. This is not possible with the sine quadrupole elements since the elements are in an angle (see Fig. 8).

V. COMMENTS ON END FIELDS

Using the same approach as above to calculate the magnetic field away from the ends of the quadrupole array, it is possible to calculate the fields in the ends. Using the same symmetry arguments, the scalar potential that described the end fields is given by

$$\phi \sim \Sigma \sin(k_x x)\sin(k_y y)\exp(-(k_x + k_y)z) \ ,$$

where the sum is over i, j, $k_x a = \pi i$, and $k_y a = \pi j$. Quadrupole-like fields are given by $i = j = 1$, in which case the field has mainly the $\cos(2\theta)$ component. By appropriately choosing the current density at the quadrupole ends, it is possible to avoid generation of fields that are not quadrupole like. The forces, by symmetry, are still aligned to the planes between cells.

TABLE III

Illustrative Designs of HTS Sine Quadrupole Magnet Array

Field graident (T/m)	40	30	20
a (m)	0.209	0.193	0.192
B_{max} (T)	8.36	5.79	3.84
A (T/m)	20	15	10
Current density (MA/m^2)	2100	2100	2100
Current density, noncopper (MA/m^2)	3000	3000	3000
Surface current density, maximum (K) (MA/m)	13.3	9.2	6.1
Total conductor thickness (cm)	0.64	0.44	0.29
Thickness of structure (cm)	2.3	1	0.45
Beam radius (m)	0.15	0.15	0.15
Field at aperture (T)	6	4.5	3
Superconductor parameters			
Conductor thickness (m)	0.00005	0.00005	0.00005
Pack current (kA)	1.05	1.05	1.05
Number of layers, maximum	127	88	58
Number of turns per layer, maximum	42	39	38
Stored energy per unit length (MJ/m)	3.24	1.32	0.58

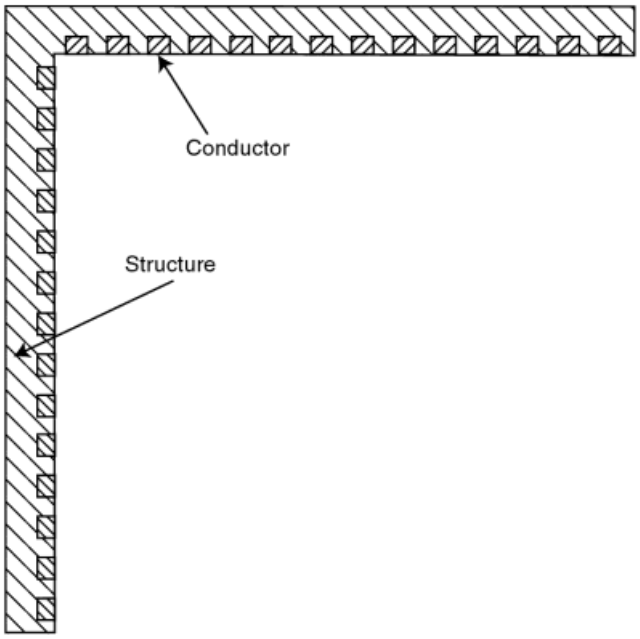

Fig. 8. Schematic diagram of a 90-deg element of a sine quadrupole magnet using HTS.

The lowest harmonic (with $i = j = 1$) generates more than the fundamental poloidal harmonic, as described above. The first four harmonics ($n = 2$, $n = 4$, $n = 8$) are shown in Fig. 9. Note that $n = 6$ is not shown since it is 0 because of symmetry.

Since different harmonics (with $i \neq 1$ and/or $j \neq 1$) have different decay rates (in the z direction) than the $i = j = 1$ case, it is not possible to zero out those undesirable harmonics the way they were cancelled in the middle of the array. It is difficult to conserve the field purity in the ends. The contributions to the field errors by the ends of the quadrupoles need to be minimized. Although substantial work has been carried out in minimizing the error fields in individual quadrupoles, this work needs to be extended to the case of quadrupole arrays.

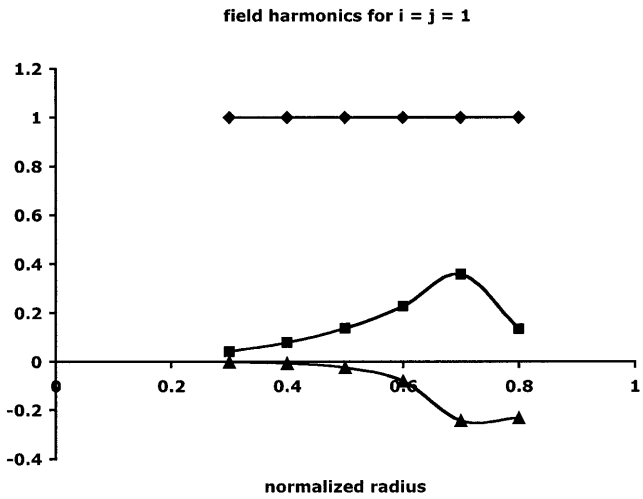

Fig. 9. Normalized field poloidal harmonics that correspond to $i = j = 1$, as a function of the normalized radius.

VI. MAGNET COSTING OF EPITAXIALLY MADE MAGNETS

The unit cost of the quadrupole magnets may be substantially decreased by utilizing the epitaxial manufacturing design described above. Instead of the complex manufacturing processes used for today's LTS magnets, modern rapid-prototyping techniques could be used.[20,21] The flat plates or 90-deg angle elements can be manufactured from either powders (as in the ARIES-ST reactor) or from raw stock. They can then be coated with the different layers to manufacture the superconductor in a process similar to that used in printed circuits and that is very easily automated. At present, nickel is being used as the substrate for tapes. It is not clear whether Inconels (nickel-based steels) could be used instead. If not, then the steel would have to be coated with a layer that serves as a diffusion barrier, onto which nickel is deposited. Alternatively, tapes can be used, which after they are manufactured can be soldered onto the structural plates. However, the use of tapes may increase the cost of the magnet because of the increased number of processes involved. Figure 10 shows a set of superconductor patterns on silver, as reported by Bromberg et al.[22]

It is estimated that the cost of the superconductor is on the order of \$200/kg, which is comparable to NbTi but is less expensive than Nb_3Sn. Since the superconductor is such a small fraction of the cross-sectional area, the cost of the magnets will be determined by the cost of the structure. The cost of the structure is being determined. It is being assumed that modern manufacturing techniques will be used. Costs as low as \$50/kg for the magnet could be feasible.[23]

The use of epitaxial methods to fabricate the magnet allows great flexibility in the choice of the cross section of the magnet and may help address those issues that were not discussed in this paper, such as the ends of the quadrupoles.

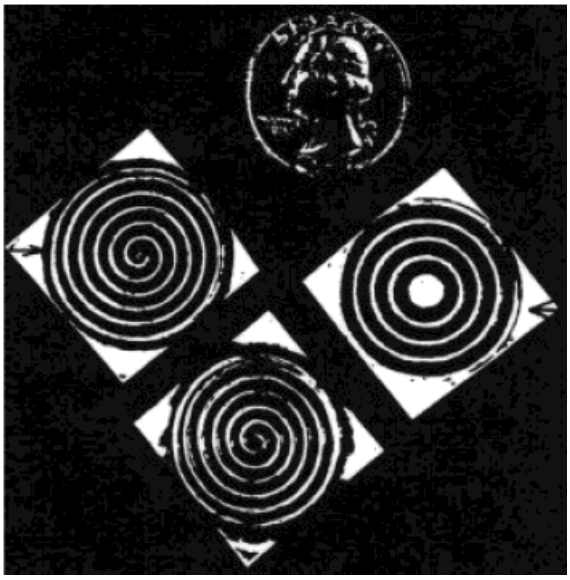

Fig. 10. Single-sided samples made of BSCCO 2212 applied on a squared-silver substrate. An American quarter-dollar is shown for comparison.

VII. SUMMARY AND CONCLUSIONS

The design of quadrupole arrays for the final focusing magnets for the heavy ion driver for inertial fusion has been scoped. Options for topology that use the fact that the quadrupoles are arranged in an array have been investigated, and it has been determined that important differences exist between single quadrupole designs and quadrupole array designs. The two types of possible magnets have been evaluated, using both HTSs and LTSs. High field purity can be achieved with these topologies. The purpose of the paper is not to develop a fully optimized, complete design but rather to scope the options for the final focusing magnets.

The use of HTS materials may be an enabling technology that spurs qualitative changes in the manufacturing of quadrupole magnet arrays. However, to be practical, substantial progress needs to occur in the areas of manufacturing (increased engineering current density, cost, and extrapolation to long lengths/areas, among others).

ACKNOWLEDGMENTS

This work was supported by U.S. Department of Energy, Office of Fusion Energy Sciences. The author acknowledges the multiple useful suggestions made by the reviewers. The manuscript is much improved because of their help.

REFERENCES

1. A. FALTENS and D. SHUMAN, "A Superconducting Quadrupole Array for Transport of Multiple High Current Beams," *Proc. 18th IEEE/NPSS Symp. Fusion Engineering*, p. 362 (1999).

2. R. B. MEINKE, A. FALTENS, R. O. BANGERTER, R. M. SCANLAN, and P. SEIDL, "Development of Quadrupole Arrays for Heavy-Ion Fusion," *Trans. Appl. Supercond.*, **10**, 192 (2000).

3. S. CASPI et al., "A Superconducting Quadrupole Magnet Array for a HIF Driver," *IEEE Trans. Appl. Supercond.*, **9**, *2* (June 1999).

4. N. MARTOVETSKY and B. MANAHAN, "Focusing Magnets for HIF Based on Racetracks," *IEEE Trans. Appl. Supercond.*, **11**, 1506 (Mar. 2001).

5. A. FALTENS and D. SHUMAN, "A Superconducting Quadrupole Array for Transport of Multiple High Current Beams," *Proc. 18th Symp. Fusion Engineering*, Albuquerque, New Mexico, October 25–29, 1999, p. 352, Institute of Electrical and Electronics Engineers/Nuclear and Plasma Sciences Society.

6. A. FALTENS et al., "Progress in the Development of Superconducting Quadrupoles for Heavy Ion Fusion," *Proc. 14th Int. Symp. Heavy Ion Fusion*, Moscow, Russia, May 26–31, 2002.

7. M. GREEN and R. BANGERTER, "Magnet and Cryostat Configurations for a Multi-Port Quadrupole Array," *IEEE Trans. Appl. Supercond.*, **11**, 1502 (Mar. 2001).

8. R. BANGERTER et al., "Parameters and Requirements of Superconducting Focusing Quadrupoles for Heavy Ion Fusion," *Proc. Applied Superconductivity Conf.*, Houston, Texas, August 2002.

9. N. MARTOVETSKY, R. MANAHAN, and A. F. LIEUKE, "Development of Superconducting Focusing Quadrupoles for Heavy Ion Drivers," *IEEE Trans. Appl. Supercond.*, **12**, 157 (2002).

10. A. CHAPIRO, R. CLOUGH, N. MERMILLIOD, and M. TAVLET, "What is Ageing? Are There Still Problems to Be Solved?," *Nucl. Instrum. Methods Phys. Res B*, **131**, x (1991).

11. K. BITTNER-ROHRHOFER, P. ROSENKRANZ, K. HUMER, H. W. WEBER, J. A. RICE, P. E. FABIAN, and N. A. MUNSHI, "Characterization of Reactor Irradiated, Organic and Inorganic Hybrid Insulation Systems for Fusion Magnets," presented at Joint Cryogenic Engineering Conf. and Int. Cryogenic Materials Conf., Madison, Wisconsin, July 16–20, 2001.

12. L. BROMBERG, M. TEKULA, L. A. EL-GUEBALY, R. MILLER, and ARIES TEAM, "Options for the Use of High Temperature Superconductor in Tokamak Fusion Reactor Designs," *Fusion Eng. Des.*, **54**, *2*, 167 (2001).

13. J. H. SCHULTZ, "Integration of High-Tc Superconductors into the Fusion Magnet Program," PSFC/RR-99-5, MIT Plasma Science and Fusion Center (Mar. 23, 1999); see also ⟨http://www.psfc.mit.edu/library/99rr/99rr005/99rr005_abs.html⟩.

14. Y. IIJIMA and K. MATSUMOTO, "High-Temperature-Superconductor Coated Conductors: Technical Progress in Japan," *Supercond. Sci. Technol.*, **13**, 68 (2000).

15. M. P. MALEY et al., "Optimization of Transport Critical Current in HTS Conductors," presented at 1996 Annual Peer Review Mtg., U.S. Department of Energy, Washington, D.C., July 31, 1996.

16. P. F. HERRMANN et al., "BSCCO Based Superconductors for Magnet Applications," *Proc. 12th Int. Symp. Superconductivity Advances in Superconductivity XII (ISS'99)*, Morioka, Japan, October 17–22, 1999, p. 730-5 (2000).

17. H. KÜPFER et al., *Z. Phys. B*, **69**, 167 (1987).

18. F. M. SAUERZOPF et al., *Phys. Rev. B*, **51**, 6002 (1995).

19. R. THOME, MIT Plasma Science and Fusion Center, Personal Communication (2001).

20. L. M. WAGANER et al., "Ultra-Low Cost Coil Fabrication Approach for ARIES-ST," *Fusion Eng. Des.*, **65**, *2*, 339 (2003).

21. W. W. ZHANG et al., "Design and Field Measurements of Printed-Circuit Quadrupoles and Dipoles," *Phys. Rev., Special Topics—Accelerators and Beams*, **3**, 12 (2000).

22. L. BROMBERG, M. SIDOROV, R. MINTS, and T. HOLESINGER, "Electrical and Thermal Behavior of Patterned Superconducting Disks," *IEEE Trans. Appl. Supercond.*, **5**, 321 (1995).

23. L. J. MASUR et al., "Industrial High Temperature Superconductors: Perspectives and Milestones," *IEEE Trans. Appl. Supercond.*, **12**, 1145 (2002).